Breaking the geometric magnetic frustration in controlled off-stoichiometric LuMn1+zO3+o compounds

Figueiras, F.G.; Karpinsky, D.; Tavares, P.B.; Soma Das; Vieira Leitao, Jose; Brück, Ekkes; Agostinho Moreira, J.; Amaral, VS

DOI
10.1039/c6cp01562j

Publication date
2016

Document Version
Accepted author manuscript

Published in
Physical Chemistry Chemical Physics

This is an Accepted Author Manuscript of an article published by RSC in the journal Physical Chemistry Chemical Physics, available online: http://dx.doi.org/10.1039/C6CP01562J

TITLE

Breaking the Geometric Magnetic Frustration in $LuMn_{1+z}O_{3+\delta}$ controlled off-Stoichiometry

AUTHOR NAMES

F. G. Figueiras [1, 2,*], *D. Karpinski* [1], *P. B. Tavares* [3], *Soma Das* [1],

J. V. Leitão [4], *E. H. Brück* [4], *J. Agostinho Moreira* [2], *V. S. Amaral* [1]

ADDRESS

[1] Physics Department & CICECO-AIM, Aveiro University, 3810-193 Aveiro, Portugal

[2] IFIMUP and IN-Institute of Nanoscience and Nanotechnology, Physics and Astronomy Department, Faculty of Sciences of University of Porto, 4169-007 Porto, Portugal

[3] Centro de Química, Trás-os-Montes & Alto-Douro University, 5001-801 Vila Real, Portugal

[4] FAME, Faculty of Applied Sciences, Delft University of Technology, Mekelweg 15, 2629 JB Delft, Netherlands

* CORRESPONDING AUTHOR:

F. G. Figueiras [1, 2,*]

* *ffigueiras@ua.pt*

ABSTRACT

This study explores controlled off-stoichiometric $LuMn_{1+z}O_{3+\delta}$ ($|\mathbf{z}| < 0.1$) compounds, intended to retain the utter $LuMnO_3$ intrinsic hexagonal symmetry and ferroelectric properties. X-ray powder diffraction measurements evidenced single phase $P6_3cm$ structure. Thermo-gravimetric experiments show a narrow impact of oxygen vacancies while distinguish a gas exchange ~700K, surprisingly lower temperature when comparing to perovskite systems. Comparison of different nominal ceramics revealed pertinent structural and magnetic properties variations owing to subtle self-doping effects. Deviations from the archetypal antiferromagnetic state were detected below ~90K suggesting local rearrangements of the nominal Mn^{3+} ions matrix, breaking the ideal geometrical spins frustration, leading to non-compensated magnetic structure.

KEYWORDS:

ferroelectric ceramics,

thermogravimetric analysis,

crystal structure,

magnetic frustration

The relevant scientific and technological interest over multiferroics [1, [2] leads to the study of a diversity of extrinsic composites and intrinsic materials, in particular based on lanthanide manganite systems ($LnMnO_3$) due to the strong spin-lattice coupling and the high sensitivity of the physical properties to doping [3]. Special attention has been given to complex magnetic ordering geometries, leading to a non-centrosymmetric crystal structures through the spin-lattice coupling, which can give rise to magnetically induced ferroelectricity, with strong magnetoelectric effect [4]. Previous studies on self-doped manganites have evidenced the subtly modification of the Mn^{3+}/Mn^{4+} ratio, crystal structure and transport properties, including magnetic and conductive behavior, besides shifting critical transitions temperatures [3]. Off-stoichiometry within a restricted amount of cationic or anionic vacancies (well below percolation threshold) has the advantage of introducing controlled electric charge doping, while minimizing ionic radius variance and preserving the same elemental chemistry, and retaining the overall structural symmetry of the stoichiometric compound. In this context, we explore the hexagonal $LuMnO_3$ system which exhibit multiferroic behavior below the Néel temperature (T_N ~90 K) where ferroelectricity coexists with a canted antiferromagnetic (c-AFM) structure arising from the geometrical frustration of the triangular lattices of Mn^{3+} ions [3]. The study of $LuMn_{1+z}O_{3+\delta}$, here reported is mainly focused on the effects of scarce cation vacancies ($-0.06 \leq \mathbf{z} \leq 0.01$), preventing percolation defects and preserving the original structural symmetry and intrinsic ferroelectric (FE) properties of the stoichiometric compound. The minor off-stoichiometry is intended to originate cation vacancies and promote subtle oxidation of neighboring Mn^{3+} ions, originating charge inhomogeneities and redistribution. These perturbations are anticipated to induce local irregularities in geometrical c-AFM frustration, as it is found in the stoichiometric compound [5]. According to Bulaevskii

model [7], an electric polarization contribution can be predicted from uncompensated triangular spins geometry; consequently, a suitable break of the ideal geometrical AFM frustration can eventually enhance multiferroic and magnetoelectric effect in the material. In order to support this idea, a more specific study of samples with nominal compositions $LuMn_{1.01}O_3$ (LuM101), $LuMn_{1.00}O_3$ (LuM100), $LuMn_{0.99}O_3$ (LuM099), $LuMn_{0.98}O_3$ (LuM098) and $LuMn_{0.94}O_3$ (LuM094) was carried out, comparing experimental results with referenced data on $LuMnO_3$ manganite.

Polycrystalline samples were prepared by sol-gel combustion method known to produce powders with low grain size distribution and homogenous composition [8]. High grade Lu_2O_3 and $Mn(NO_3)_2{\cdot}4H_2O$ compounds were used as precursors. Effective formation of the hexagonal phase was achieved after calcination at 600 ^oC for 4 h, followed by grinding, sieving, pressing into pellets, sintering under air and quenched to room temperature. Samples LuM100; LuM099 and LuM094 were sintered at ~900 ^oC during 96 h. Samples LuM101 and LuM098 were additionally sintered at 1300 ^oC during 68 h, then recovering the ~900 ^oC annealing for 24 h. SEM observation and EDS analysis were performed with a *FEI Quanta 400* (W filament) with an *EDS/EDAX* detector. Rutherford Backscattering (RBS) and Proton Induced X-Ray Emission (PIXE) spectrograms were simultaneously acquired. Samples were irradiated with 2 MeV protons focused in 3x4 μm^2 and sweeping thru 1.5x1.5 mm^2, having found no composition heterogeneities or contaminants. Thermogravimetric analyses (TGA) were carried out using a *Setsys Evolution 175*0 (*Setaram*) under O_2 flow from room temperature to 400 K at 10 K/min, twice cycled up to 1150 K and once up to 1800 K at 2 K/min rate. Photoluminescence spectra were recorded at 12 and 300 K with a *Horiba TRIAX 320* coupled in front face acquisition mode to a *Hamamatsu R928* photomultiplier, using a 450 W Xe arc lamp as excitation source. X-ray diffraction was

performed in a *Panalytical X´Pert Pro* equipped with *X'Celerator* detector and secondary monochromator detector using Cu K_α radiation (λ = 1.5418 Å). Rietveld refinements were performed using *FullProf* software [9]. Magnetization measurements from 5 to 300 K up to 10 Tesla used a *Cryogenic Ltd.* VSM system, whereas for measurements up to 400 K a *Quantum Design MPMS-XL* SQUID system was used [10].

The samples composition was checked by SEM/EDS and corroborated by comparison with the results from RBS/PIXE techniques. No significant traces of contaminants were found. The atomic ratio |Mn|/|Lu| obtained is consistent with the intended nominal composition expressed within the horizontal error bars expressed in figure 1a. XRD patterns reveal that presence of possible spurious phases like Lu_2MnO_5 or Mn_3O_4 are below accountable limit (<0.5%). Nevertheless, additional verification using luminescence measurements evidence some residual traces of Lu_2O_3 phase in samples LuM094 and LuM099. As such, for the same sintering conditions, the self-doped LuM099 and LuM094 samples did not attained similar crystallographic quality and chemical homogeneity as found in the LuM100 stoichiometric compound, subsequently, samples LuM101 and LuM098 were subjected to additional sintering. The Rietveld analysis of the obtained XRD data was successfully performed assuming single phase structure for each compound, with the characteristic hexagonal space group $P6_3cm$ (185), as exemplified in figure 1b, with typical quality factors $R_p < 5$, $R_{wp} < 7$ and $R_{exp} < 3$. Estimated mean crystallites size for the samples LuM101 and LuM098 is ~93 nm, and for the samples LuM100, LuM099 and LuM094 is ~ 55 nm. The comparison of the calculated ***a*** and ***c*** lattice parameters and unit cell volume of the samples with several referenced data for nominal $LuMnO_3$ compounds [5, 11-21] is shown in figure 1. The dispersion of cell parameter values (~0.03 % variance in ***a*** and ***c***) published for this system can be understood from eventual slight off-stoichiometry (**z**,

δ) which has not been considered, a normal consequence of the different synthesis methods, precursors quality, sintering and annealing conditions.

The cell parameters of the nominal $LuMnO_3$ compounds closer to stoichiometry as LuM100 and LuMn099 are consistent with the values reported by Lee [5], Van Aken [11] or Ghosh [12]. Sample LuM101 reveals some contraction, whereas for samples LuM094 and LuM098 is perceptible a volume expansion of the unit cell due to a pronounced extension of ***a*** parameter. This effect is compatible with the manifestation of Mn vacancies and anionic repulsion, promoting a slight elongation of Mn–O bonds located in the basal plane. Such interpretation is also plausible to elucidate the structural spread found in several nominal compounds supposed as stoichiometric [13-21].

The extensive work developed by Dabrowski *et al*. [22] supports the strong decrease of the oxygen diffusion and intake in pseudo perovskite manganite systems with the decrease of the A-site element ionic radius. For the extreme case of lutetium manganite, the oxygen excess could be extrapolated to $\delta \approx +0.01$ for samples sintered at 1200 K and $\delta \approx -0.005$ for 1600 K [22]. However, more recent studies [23, 24] suggest oxygen thermodynamics modeled for perovskite systems should differ significantly for the hexagonal structures, due to the lower ionic density and layered MnO_5 bipyramidal arrangements. In order to access the relative impact arising from anionic vacancies (**δ**) in the $LuMnO_3$ system, thermogravimetry (TG) experiments were performed. Figure 2a confirms that by cycling the sample up to 1150 K, the observed mass variations are completely reversible and due to oxygen exchange. Figure 2b shows that quenching the samples from above 1400 K can lead to a slight $\delta \approx -0.002$; also suggesting that **δ** variations can be reversed after annealing treatments reaching 1300 K. These TG experiments ultimately enable to constrain $|\delta| < 0.004$ for samples under study. Besides the normal dehydration at 400-500 K, an additional and relevant feature to point out is

the partial mass/oxygen exchange observed between 600 and 700 K, surprisingly ~200 K below the typical temperatures at which such ionic processes arise in perovskite manganite [22].

The Lu-Mn-O phase diagram [25] has some similarities to the perovskite manganite compounds [26] and can also tolerate a limited deficit of A or B-site vacancies well below percolation limit without compromising the stability of the hexagonal structure. The two main mechanisms to preserve charge neutrality of a doped system (**z**) are considered: partial oxidation of Mn ions and/or formation of oxygen vacancies [27]. In particular, charge compensation mechanisms due to each Mn deficit lead up to 3 valence electrons default which, for **δ** ~0, in the pseudo-perovskite systems can impinge three Mn^{4+} ions. However, for the hexagonal system, no volume contraction is evident as predictable from the occurrence of smaller Mn^{4+}–O^{2-} bonds. In fact, the bipyramid crystal field (MnO_5) have a narrow splitting of the d-orbital energies, hence are less Jahn-Teller active and less prompt to form Mn^{4+} ions, than the octahedral cages (MnO_6) [28]. In addition to localized charge anomalies due crystallographic defects or grain boundaries, it is also conceivably that the new charge equilibrium could be unevenly dispersed through Mn^{3+} ions matrix; in fact, charges redistribution are not necessarily homogeneous, the $P6_3cm$ space group allows some subtle asymmetries for the six different Mn ions positions in the cell structure, each can slight differ in hybridization and intrinsic magnetic moment. These charges redistributions should reflect in the magnetic properties of the samples. In figure 3 and 4 is possible to compare some pertinent differences between the magnetic responses of the compounds. Albeit the small off-stoichiometry and spatial dispersion of cationic vacancies, the ensuing electronic perturbations are sufficient to modify the delicate balance of the compensated AFM matrix.

Magnetization measurements as function of temperature are represented in figure 3; the compounds with Mn deficit (LuM094, LuM098, LuM099) clearly exhibit a smoothing of the anomaly of the M(T) curve at the expected AFM magnetic phase transition, near $\mathbf{T}_N$ ~90 K, when compared to the more conventional behavior of the LuM100 and LuM101 samples. Pronounced anomalies in the curves allow us to detect the Nèel temperature. Moreover, small anomalies observed between 25 and 50 K attest additional magnetic rearrangements arising from complex competition between antiferromagnetic interactions, as it was discussed by Das [29]. For the paramagnetic regime considered above 100 K, it is possible to perform (in the range 150-250 K) a basic approach to the conventional Curie Weiss model $\{\chi = \mathbf{C}/(\mathbf{T}\text{-}\boldsymbol{\Theta})\}$ enabling the calculation of the effective magnetic moment ($\boldsymbol{\mu}_{eff}$) and of parameter $\boldsymbol{\Theta}$, which denotes a clue of the antiferromagnetic exchange interaction. For the compounds closer to stoichiometry, LuM099, LuM100 and LuM101, the $\boldsymbol{\Theta}$ values are very similar (~ -370 K) and $\boldsymbol{\mu}_{eff}$ ~4.9 μ_B/Mn, which agrees with the expected value for high spin configuration of Mn^{3+}, with $\boldsymbol{S}$ = 2 [30]. For the sample designated LuM098 there is a manifest deviation from the linear paramagnetic behavior, surprisingly, $\boldsymbol{\mu}_{eff}$ approaching ~5.6 μ_B/Mn ion at room temperature and, particularly, $\boldsymbol{\Theta}$ <-550 K, suggesting a notable strengthening of antiferromagnetic interactions. The deviation from the linear expected Curie-Weiss law evidence the stabilization of complex magnetic cluster-like behavior well above $\mathbf{T}_{Neel}$.

Magnetization measurements as function of external field shown in figure 4, revealed hysteresis loops in the self-doped samples with significant remanence and coercive fields, reaching 0.005 emu/g and 0.02 T for sample LuM098 and 0.025 emu/g and 0.1 T for sample LuM101; substantiating the presence of some weak ferromagnetic component, not observable in the AFM stoichiometric LuM100 compound.

In the present hexagonal manganite system, the polaronic exchange mechanism is lessen by the 120º angles in basal planes and is ruled out in the perpendicular axis. The super-exchange interaction is dominant in the regular spatial charge distribution of adjacent Mn^{3+}, dictating an antiferromagnetic order [5]. Nevertheless, slight off-stoichiometry overrides the strict overall symmetry rules, each vacancy imposes a local inhomogeneity and a slight redistribution of spatial charge, hence disturbing the conformed Mn^{3+} orbital clouds position and symmetry. Moreover the disseminated presence of vacancies can act simply as pinning dwells for domain walls [31] or even magnetic clusters [32, 33].

We observe that the $LuMnO_3$ hexagonal phase can be tolerant to a narrow cationic off-stoichiometry ($|\mathbf{z}| < 0.1$) and minor oxygen adjustments ($|\boldsymbol{\delta}| < 0.005$) without substantial structural changes or phase segregation. In addition, TG experiments revealed an enhanced mass exchange at ~500 K, which is thermodynamically 300º lower than typically found in perovskite systems. Self-doping leads to a predictable ionic balance with slight oxidation of Mn^{3+} ions, resulting a noteworthy perturbation of magnetic triangular ordering, hence partially breaking the antiferromagnetic geometric frustration found below $T_{Néel}$ ascribed for the stoichiometric compound. Materials modification by self-doping suits a valid experimental approach to enhance multiferroic and magnetoelectric properties. Comparing several published works ascribed as $LuMnO_3$, it becomes patent that the spread of structural and magnetic results can be understood within the high sensitivity of this system to very small composition variations.

ACKNOWLEDGEMENTS

This work was developed within the scope of the project CICECO-Aveiro Institute of Materials, POCI-01-0145-FEDER-007679 (FCT Ref. UID/CTM/50011/2013), financed by national funds through the FCT/MEC and when appropriate co-financed by FEDER under the PT2020 Partnership Agreement. We would like to thank the financial support from the FCT project PTDC/FIS/10541/2008 "MULTIFOX", F. F. author SFRH/BD/25011/2005 and SFRH/BPD/80663/2011 grants. This work was also supported by Fundação para a Ciência e Tecnologia, through the Project PTDC/FIS-NAN/0533/2012 and by QREN, through the Project Norte-070124-FEDER-000070 Nanomateriais Multifuncionais.

REFERENCES

[1] J. Kreisel, M. Kenzelmann, EPN **40/5**, (2009) 17-20.

[2] D. Khomskii, Physics **2**, (2009) 20.

[3] F. Figueiras, J.P. Araujo, V.S. Amaral, P.B. Tavares, J.B. Sousa, J.M. Vieira, J. Magn. Magn. Mater. **272–276**, (2004) 1753.

[4] S. W. Cheong & M. Mostovoy, Nat. Mater. **6**, (2007) 13–20.

[5] S. Lee, A. Pirogov, M. Kang, K.-H. Jang, M. Yonemura, T. Kamiyama, S.-W. Cheong, F. Gozzo, N. Shin, H. Kimura, Y. Noda, J.-G. Park, Nature **451**, (2008) 805.

[6] L. Balents, Nature **464** (2010) 199-208.

[7] L. N. Bulaevskii, C. D. Batista, M. V. Mostovoy, D. I. Khomskii, Phys. Rev. B **78**, (2008) 024402.

[8] D. A. Fumo, J. R. Jurado, A. M. Segadães, J. R. Frade, Mat. Res. Bulletin, Vol. **32**, 10, (1997) 1459-1470.

[9] J. Rodriguez-Carvajal, Physica B, **192**, (1993) 55.

[10] J. H. Belo, A.M. Pereira, J. Ventura, G.N.P. Oliveira, P. B. Tavares, L. Fernandes, P. A. Algarabel, C. Magen, L. Morellon, M.R. Ibarra, J. Alloy Compd. **529** (2012) 89-95.

[11] Bas B. van Aken, A. Meetsma, T. T. M. Palstra, Acta Cryst. **E57**, (2001) 101-103.

[12] A. Ghosh, J. R. Sahu, S. V. Bhat, C.N.R. Rao, Solid State Sciences **11**, (2009) 1639–1642.

[13] K. Yoshii and H. Abe, J. Solid State Chem. **165**, (2002) 131–135.

[14] H. L. Yakel, W. C. Koehler, E. F. Bertaut, E. F. Forrat, Acta Cryst. **16**, (1963) 957.

[15] K. Uusi-Esko, J. Malm, N. Imamura, H. Yamauchi, M. Karppinen, Mater. Chem. Phys. **112**, (2008) 1029–1034.

[16] N. Imamura, M. Karppinen, H. Fjellvag, H.Yamauchi, Solid State Commun. **140**, (2006) 386-390.

[17] H. J. Lewtas, A. T. Boothroyd, M. Rotter, D. Prabhakaran, H. Müller, M. D. Le, B. Roessli, J. Gavilano, P. Bourges, Phys. Rev. B **82** (2010) 184420.

[18] T. Katsufuji, M. Masaki, A. Machida, M. Moritomo, K. Kato, E. Nishibori, M. Takata, M. Sakata, K. Ohoyama, K. Kitazawa, H. Takagi, Phys. Rev. B **66**, (2002) 134434.

[19] T. Katsufuji, S. Mori, M. Masaki, Y. Moritomo, N. Yamamoto, H. Takagi, Phys. Rev. B **64**, (2001) 104419.

[20] F.C. Tsao, P.J. Huang, C.C. Yang, S.Y. Wu, W.-H. Li, K.C. Lee, J.W. Lynn, H.C. Ku, J. Magn. Magn. Mater. **272–276**, (2004) 1778–1779.

[21] C. T. Wu, B. N. Lin, H. C. Ku and Y. Y. Hsu, Chinese J. Phys. **41**, 6 (2003) 652-662.

[22] B. Dabrowski, S. Kolesnik ,A. Baszczukb, O. Chmaissem, T. Maxwell, J. Mais, J. Solid State Chem. **178**, (2005) 629–637.

[23] S Remsen, B. Dabrowski, Chem. Mater. **23**, (2011) 3818–3827

[24] Y. R.-Barcelay, J. Agostinho Moreira, A. Almeida, J. P. de la Cruz, Thin Solid Films **520**, (2012) 1734–1739

[25] V. F. Balakirev, L. B. Vedmid', A. M. Yankin, Yu. V. Golikov, Doklady Physical Chemistry **389**, 4–6, (2003) 87–89.

[26] V.A. Khomchenko, I.O. Troyanchuk, H. Szymczak, Mater. Chem. Phys. **111**, (2008) 154.

[27] I. Gelard, N. Jehanathan, H. Roussel, S. Gariglio, O.I. Lebedev, G.V. Tendeloo, C. Dubourdieu, Chem. Mat. **23**, (2011) 1232–1238.

[28] C. Y. Ren, Phys. Rev. B **79**, (2009) 125113.

[29] R. Das, A. Jaiswal, S. Adyanthaya, P. Poddar, J. Phys. Chem. C **114**, (2010) 12104–12109.

[30] J. M. D. Coey, M. Viret and S. von Molnar, Adv. In Phys. **48**, 2 (1999) 167.

[31] M. Lilienblum, T. Lottermoser, S. Manz, S. M. Selbach, A. Cano, M. Fiebig, Nat. Phys. **11** (2015) 1070-1074.

[32] D. P. Chen, Y. Du, X. L. Wang, Z. X. Cheng, S. X. Dou, Z. W. Lin, J. G. Zhu, B. Xu, J. App. Phys. **111**, 07D913 (2012)

[33] C. Zhong, Q. Jiang, H. Zhang, X. Jiang, Appl. Phys. Lett. **94**, (2009) 224107.

FIGURES CAPTIONS:

Figure 1: a) Comparison between samples composition and cell parameters obtained for the series of samples LuM- “094”; “098”; “099”; "100"; "101" respectively and from referenced data [5, 11-21]. **b)** Example of XRD and Rietveld refinement of sample LuM098.

Figure 2: TG measurements of sample LuM101 in low pressure O_2 atmosphere, **a)** double cycling to 1150 K; **b)** single cycle to 1800 K.

Figure 3: Magnetic measurements as function of temperature for the series of samples: a) $\boldsymbol{B}/\boldsymbol{M}$ vs. $\mathbf{T}$ and b) $d\boldsymbol{M}/d\mathbf{T}$. Inset: Detail of Curie-Weiss fits and calculated parameters.

Figure 4: Comparison of magnetization ($\boldsymbol{M}$) as function of magnetic field ($\boldsymbol{B}$) at different temperatures for samples LuM **a)** -098, **b)** -100, **c)** -101. Respective insets zoom the behavior at low fields subtracted from the linear PM contribution.

Figure(s)

Click here to download high resolution image

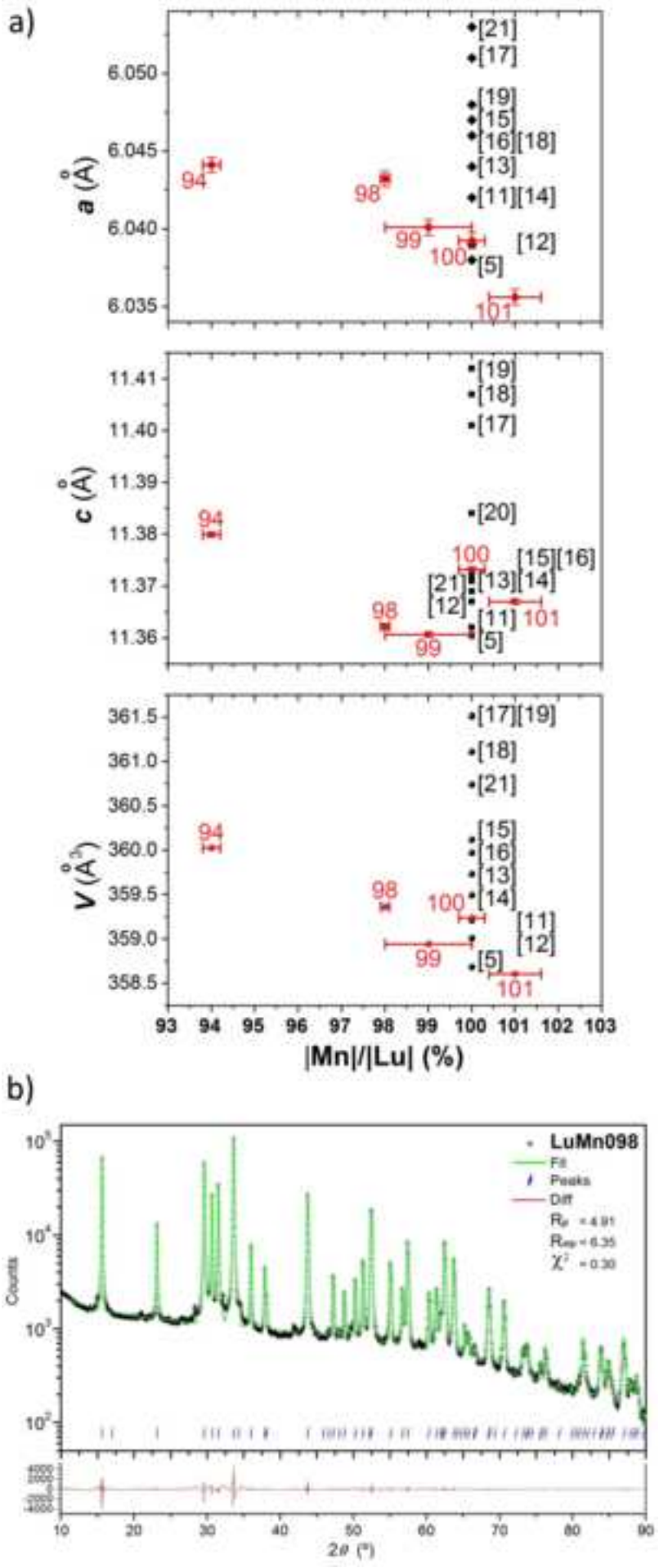

Figure(s)

Click here to download high resolution image

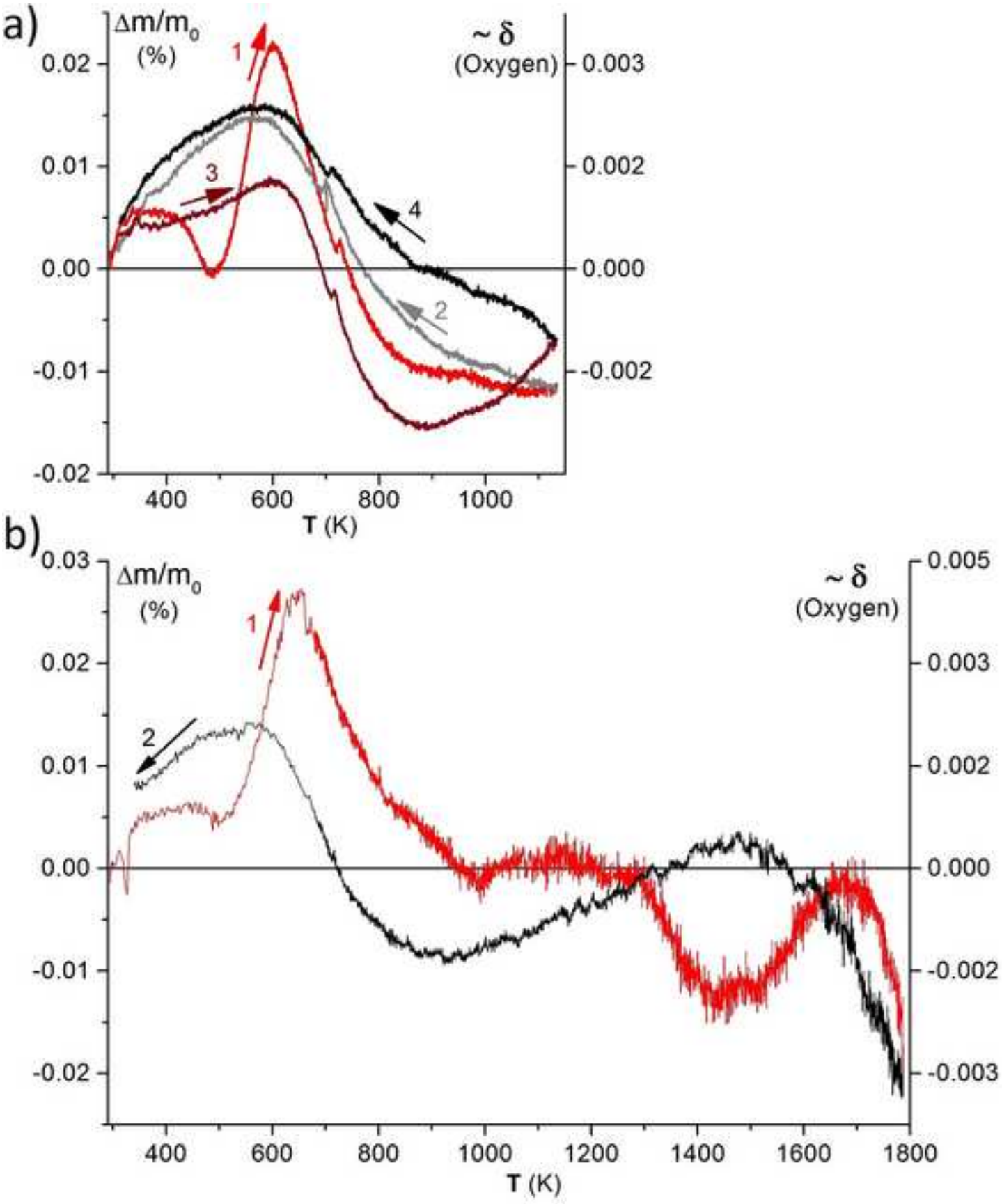

Figure(s)

Click here to download high resolution image

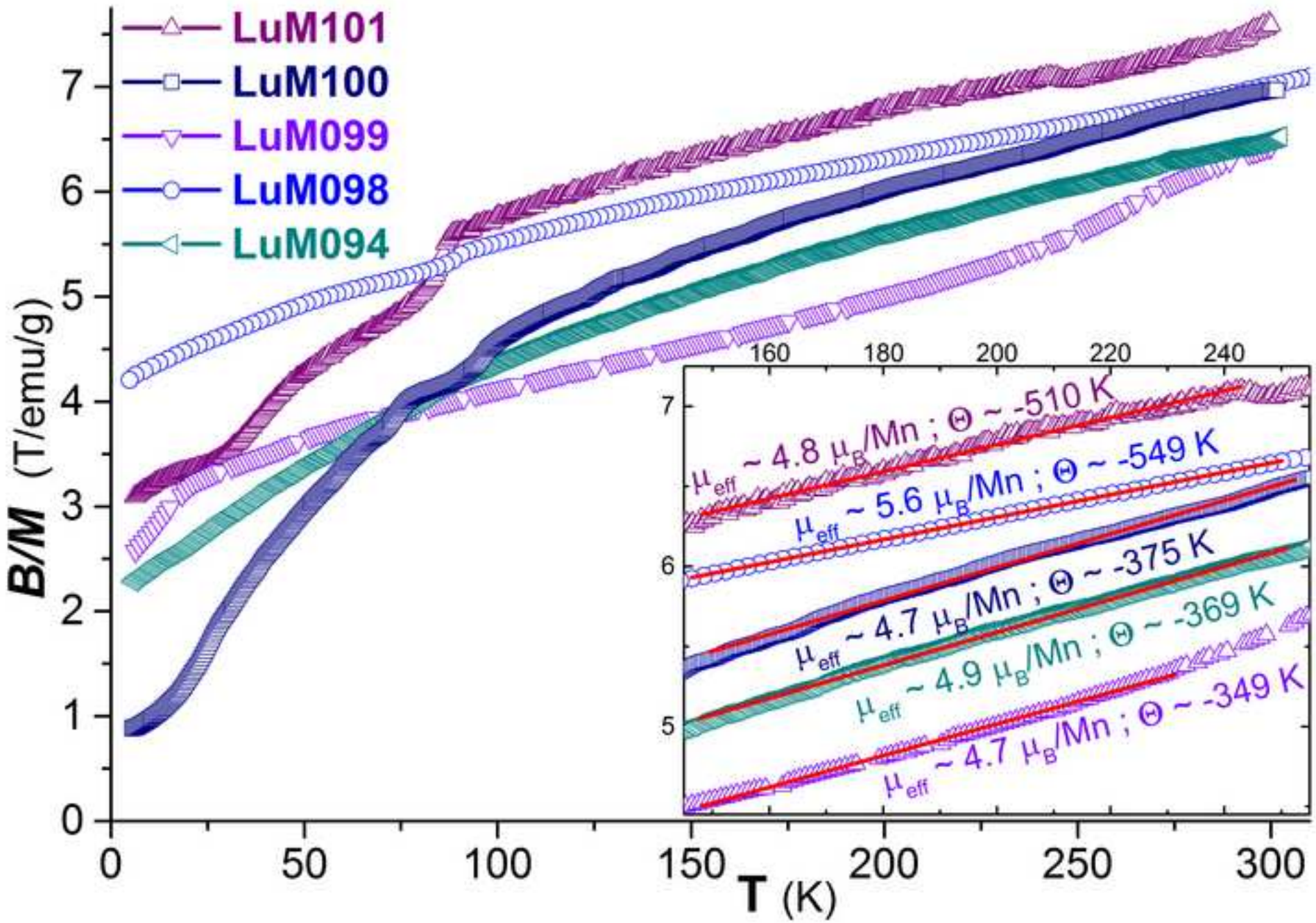

Figure(s)

Click here to download high resolution image